Wear 530–531 (2023) 205038

Contents lists available at ScienceDirect

Wear

journal homepage: www.elsevier.com/locate/wear

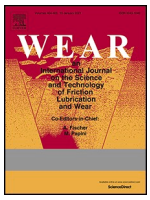

Design, wheel-rail interaction and testing of an innovative reinforced smooth transition insulated rail joint

Gianluca Megna [a,*], Andrea Bracciali [a], Nirmal K. Mandal [b]

[a] Department of Industrial Engineering, Università degli Studi di Firenze, Firenze, Italy
[b] Central Queensland University, Centre for Railway Engineering, Queensland, 4702, Australia

ARTICLE INFO

Keywords:
Insulated rail joints
Wheel-rail interaction
Impact forces
Fatigue failures
Derailment
Finite element modelling

ABSTRACT

Insulated Railway Joints (IRJ) fail mainly because of repeated shocks in the end post region, characterized by a largely reduced stiffness, causing loss of insulation (lipping), star cracks in the fishbolt holes and eventually broken rails leading to possible derailments. Laboratory tests to qualify IRJs are inadequate as they do not replicate impact loads. An innovative, reinforced joint named ABJ, made of forged shallow depth switch rails with a long, inclined cut and a thick reinforcing steel baseplate is introduced in the paper. It doesn't show a dip angle in the transition area, resulting in smooth wheel-rail transition forces preventing rail damage, impact noise, vibrations and ballast deterioration. It is designed to be laid on standard sleepers and it can be installed on standard track. An innovative cable routing allows plain and continuous tamping operations optimizing track behaviour and degradation in the long term. Impact noise typical of rail joints is eliminated and the estimated life is theoretically infinite. The paper describes the static and dynamic behaviour of the ABJ as well as the wheel-rail interaction obtained by numerical simulations and a partial full-scale validation of the new joint.

1. Introduction

Continuous Welded Rail (CWR) is widespread in railway tracks and the number of rails that are mechanically jointed has significantly reduced over the years. However, electrically insulated joints for signalling purposes, called Insulated Rail Joints (IRJ), are still popular as they are needed to define track circuits.

Conventional IRJs are assembled starting from two square-cut (90°) and web drilled rails, then the gap is filled with an around 5 mm-thick nylon slice, called "end post", and the rails are connected using fishplates and fishbolts through the proper use of electrically insulating elements. Regardless of the shape of the fishplates, the gap leads to a reduction in the vertical stiffness compared to the standard rail that generates a dip angle at the wheel pass-by leading to shocks that may reduce expected service life down to 12–18 months, corresponding to about 200 MGT (Million Gross Tons) [1,2].

The presence of electrical cables needed to connect the track circuitry makes the standard ballasted track maintenance procedures, i.e. tamping, very difficult in practice, further reducing IRJ life as shown in Ref. [3] where the effect of unsupported sleepers, i.e. hanging sleepers, is analysed.

Because of shocks, large impulse noise peaks [4] and high dynamics forces [5] are generated by each passing wheel, causing vibrations and damaging ballast. The detrimental effects of dynamic forces at IRJs on the fatigue life of rail fastenings are shown in Ref. [6]. Shocks ultimately result in joint failure with different modes, including plastic flow (Fig. 1) and eventually to the contact ("lipping") of rail ends, vanishing the required insulation of the joint and increasing the maintenance costs [2].

If CWR axial loads are relatively easily estimated from the rail cross section area and the maximum temperature difference from the stress-free condition, vertical service loads are much less predictable.

The global uncertainty on the actual behaviour of in service IRJs is highlighted by the large differences existing in the standards adopted by several infrastructure managers to qualify IRJs. While an extensive comparison of these standards goes beyond the goal of this paper, a small but meaningful set of national specifications including the next European standard [7] highlights (Fig. 2) that while some countries try to replicate the vertical behaviour in service (in one case with two vertical actuators imposing a sort of "passing load"), some others simply introduce "conventional" or "equivalent" loads.

It can be seen that both pull-apart and fatigue tests vary largely in

* Corresponding author.
E-mail address: gianluca.megna@unifi.it (G. Megna).

https://doi.org/10.1016/j.wear.2023.205038
Received 27 February 2023; Received in revised form 1 June 2023; Accepted 26 June 2023
Available online 28 June 2023

Fig. 1. IRJ with heavy plastic deformation generated by dynamic forces at each wheel passage. Insulating elements are clearly damaged (Photo by the authors).

terms of values and even in terms of testing conduction details. This indirectly proves the inadequacy of any static testing layout to reliably assess the probability of survival of a joint when installed in real track subjected to impacts in the end post area. None of the joints qualified with these tests is exempt from cracks, even those that are tested with tension values unrealistic for CWR. Increasing acceptance values is not the right way to ensure a longer IRJ life.

As any laboratory test has poor significance for the estimation of the service life of a given joint, only tests in a real environment can effectively determine whether a given architecture is valid or not.

Cracks in the rail, typically arising from fishbolt holes ("star cracks" or defect 135 according to rail defect catalogues), may even progress until portions of the rails are detached. In some particularly unlucky circumstances, this led to relevant railway accidents, such as those that occurred in the UK in 1967 (Hither Green, 39 fatalities [8]) and in Italy in 2018 (Pioltello, 3 fatalities [9]) (Fig. 3).

To reduce as much as possible the risk of failures, several approaches were used. A well-known remedy to reduce largely the risk of star crack nucleation is the "cold bolt expansion" technique, while widened sleepers were adopted to make the joint "supported" instead of "suspended". Several transducers (passive, electrical, optical) were developed to detect joint debonding or gap widening. None of these measures then prevents the problem, and non-destructive monitoring techniques can only intercept developing cracks before they reach an (uncertain) critical size.

Fig. 3. Broken IRJ in Hither Green, UK (1967) and in Pioltello, Italy (2018). (For interpretation of the references to colour in this figure legend, the reader is referred to the Web version of this article.)

As the fishbolt holes are hidden by the fishplates, the only way to inspect IRJs is the use of ultrasonic testing. The same technique is used to verify the bonding status of an IRJ as described in Ref. [10], while on-board monitoring based on axlebox acceleration (ABA) is shown in Ref. [11]. Speed restrictions proved to be poorly effective in reducing the stresses on the fishplates of IRJs installed on heavy haul network [12].

Attempts to improve the mechanical behaviour of IRJ were made without definitive results. A parametric study [13] including different track configurations shows that stresses in rail head are not significantly affected by track stiffness, by the IRJ position (suspended or supported) or by the shape, i.e. the stiffness, of the fishplates. External reinforcements were studied to reduce joint deflection [14], while railhead shape optimization to reduce stress levels was simulated [15] and tested [16]. The concept of a sleeper embedded joint is shown in Ref. [17].

The most obvious solution to reduce impacts is the use of an inclined cut between the rails to perform a progressive transition such as those used in expansion joints and switch blades (Fig. 4). In these devices the load transfer is smooth, and damages occur less frequently as confirmed e.g. by the much larger number of studies about damages introduced at crossing compared to studies about switch and stock rail damages [18, 19].

Inclined cuts can be implemented with severe limitations due to the small rail web thickness. Angles between 60° and 90° were studied in Ref. [20] using Finite Element Analysis (FEA), showing little influence on the behaviour of the joint in terms of peak stresses and strains, as the resulting transition is too short to avoid impacts. More relevant results were obtained by introducing a fillet at the rail edges. The behaviour of a standard 90° cut joint and a 75° cut joint was evaluated in Ref. [21], showing that there are no major advantages in using the inclined cut, while tests performed on 30° and 45° cut joints [22] showed better

Country	Standard	Static test force [kN]	Wheel load [kN]	Force [kN]	Joint support distance [mm]	Max bending [kNm]	# cycles [*10⁶]	Freq. [Hz]	Note
ITA	RFI TCAR SF AR 07 008 A	F_h=1500	N/A	F_v=30÷300	1100	*71.25*	2	3÷5	
EU	prEN 16843:2019	F_h=1450 [1]	125	F_v=5÷*167.6* [2]	924 ≤ Ls ≤ 1268 [3]	39.8 [4]	3	3÷10	
TUR	TCDD IRC: 2017	F_h=2000	N/A	F_v=15÷200	1000	*50*	5	≤ 20	
ESP	ET 03.360.109.7	F_h=1290	N/A	F_v=39.2÷172.87	640	*27.7* [5] (biaxial test)	3	6÷10	Hardened railhead ends
AUS	AS 1085.12-2002	F_h=1130 F_v=210 [6] (biaxial test)	N/A	F_v=1100 (static) [7] F_v=10÷245 (fatigue)[8]	600 (static) [9] 1100 (fatigue) [10]	*165* (static) *67.4* (fatigue)	3	5÷10	Hardened railhead ends
GBR	RT/CE/S/023 1996 [11]	F_h=700 (1 h)	N/A	F_v=5÷205 F_h=460 (const.)	1286 [12]	*46.5* [13]	2	1÷10	

[1] Calculated for a 60E1 rail, with ΔT=50 °C, safety coefficient γs=1.5.
[2] Calculated from Eqn. (9) with support distance L_s=1100 mm and longitudinal distance between vertical supports L_w=150 mm.
[3] Calculated for a typical fishplate with L_f=580 mm and a rail height of 172 mm with Eqn. (8).
[4] Taken from table G.1 (for a 60E1 rail, suspended joint, maximum vertical deflection of the track w_{max}=1.5 mm).
[5] A total of 1826 cycles of traction/compression are applied with -45/+45 kN (spring + autumn), -60/+30 kN (summer), -30/+60 kN (winter).
[6] For a 60 kg/m rail according to Table D1 (axial load 1280 kN and vertical load 300 kN for a 68 kg/m).
[7] Called "Load deflection test" with max deflection of 20 mm for 60 kg/m rail. It further requires reaching 1900 kN or failure.
[8] Fatigue load for 60 kg/m rail (10÷290 kN for 68 kg/m rail)
[9] For "Load deflection test".
[10] For fatigue test.
[11] Only values for Classes of joint A&B are listed here.
[12] Longitudinal distance between vertical supports L_2=400 mm
[13] Actuators A&B supply a variable load in the range 5÷205 kN in counterphase. Nevertheless, the bending moment remains the same when the two forces overlap.

Fig. 2. Comparison of some national and international standards on IRJ acceptance tests.

Fig. 4. Above: an expansion joint (source: Internet). Below: Switch rail/stock rail pair of a heavily loaded turnout (Photo A. Bracciali, Florence, July 09, 2022).

results in terms of peak acceleration and noise level respect to squared IRJ, but the advantages are nevertheless still limited.

The first option to "artificially" increase the web width is to laterally bend standard rails that were used in the past for expansion joints. Machining of the bent rails is then needed to restore the original railhead shape. To the authors' knowledge, no IRJ was produced by using this solution.

Another possibility to create a longer ("scarf" or "mitre") inclined cut is to machine special rails with thicker web used for bridge expansion joints or switch rails. Plaut et al. [23] studied the static behaviour of a tapered joint with two different angles, 2.4° (cut length 690 mm) and 8° (cut length 200 mm), made of full depth symmetric switch rails, i.e. 136 TW according to AREMA standard getting better performances in terms of deflections, bending moments and shear stresses in the adhesive layers respect to conventional IRJs, but some concerns were expressed about the costs of using such rails. Prototypes were installed on a test track [24] and on main lines [25], but a comprehensive description of the test results or a detailed analysis of the wheel-joint interaction was not found in the literature.

A reinforced, fishplate-free innovative joint, called Absolutely Better Joint (or ABJ for short) is introduced in this paper. It is characterized by a very inclined (<3°) tapered cut, shallow depth switch rails and a robust thick joint cover. The work aims to compare ABJs to conventional IRJs investigating wheel-rail interaction features, to confirm that a progressive and smooth transition leads to dramatic advantages in terms of joint integrity and service life.

The present paper is the extended version of the paper presented at Contact Mechanics 2022 in Melbourne [26]. The ABJ concept and structural validation are described in section 2, while simulations performed to investigate static/dynamic behaviour and wheel-rail interaction are shown in section 3. Tests conducted on the prototype are described in section 4, and then conclusions and further developments follow.

2. Concept, design and structural validation of the ABJ

The patent pending [27] ABJ is assembled from standard components with limited machining operations and with manufacturing sequences that are very similar to conventional IRJs.

The joint described in this paper (Fig. 5) was obtained starting from 60E1A2 [28] forged shallow depth switch rails, which are manufactured with thicker web (40 mm instead of 16.5 mm) and shallower depth (134 mm instead of 172 mm) than the mating standard 60E1 rail. The switch rails are machined, glued with an intermediate insulating fibreglass layer and connected by six lockbolts with thin insulating short tubes made of advanced polymers. This sub-assembly is then glued and bolted to the lower reinforcing plate with another insulating layer in between. Further locking elements are present in heavy duty versions. In a particularly attractive architecture, bolts also work as electrical conductors for track circuitry completely freeing the area for tamping.

The ABJ is highly modular, as the number of lockbolts, the length of the stiffening plate and its connection to the rails can be adapted to specific needs. As an example, underground metro tracks are subjected to lower mechanical and thermal stresses, and "light" versions of ABJ are feasible.

The ABJ has the following advantages.

- the long and very shallow (<3°) cut results in a "smooth" transition about 500 mm long;
- the reinforcing plate (joint cover) is connected under the switch rails foot resulting in a continuously supported joint with high bending stiffness;
- conventional IRJ fishplates are suppressed, freeing the area below the railhead and allowing the uninterrupted operation of tamping machines rail lifting units;
- it is designed to use standard a standard track (same rail fasteners, same sleepers, same sleeper spacing);
- the use of advanced insulating material allows reducing fishbolt hole diameter, allowing a larger number of bolts;
- the ABJ have a flexible design, in the sense that the number of bolts can be either even or odd according to the design specifications;
- the arrangement with conducting bolts completely frees the tamping area, allowing an unprecedented track maintenance ease.

Finite element (FEA) numerical analyses are extensively used in engineering for the assessment of mechanical behaviour or mechanical structures. FEA is used in this project to validate the ABJ design in terms of strength in pull-apart and bending (fatigue) conditions.

Joints are normally made by using a single technique, e.g. welding, bolting or bonding. Design rules for these joints are quite established and many practical guidelines can be found. On the opposite, the design of "hybrid joints" obtained by mixing different techniques is much less documented in technical literature. Typically, the use of bolted-bonded joints is limited to small or lightly loaded joints, such as those obtained starting from polymeric or composite materials. To satisfy the requested strength of IRJs, neither bolts nor glue can be applied alone but no design rules were found for heavily loaded, large bolted-bonded joints.

Most of the literature is based on experimental tests on small

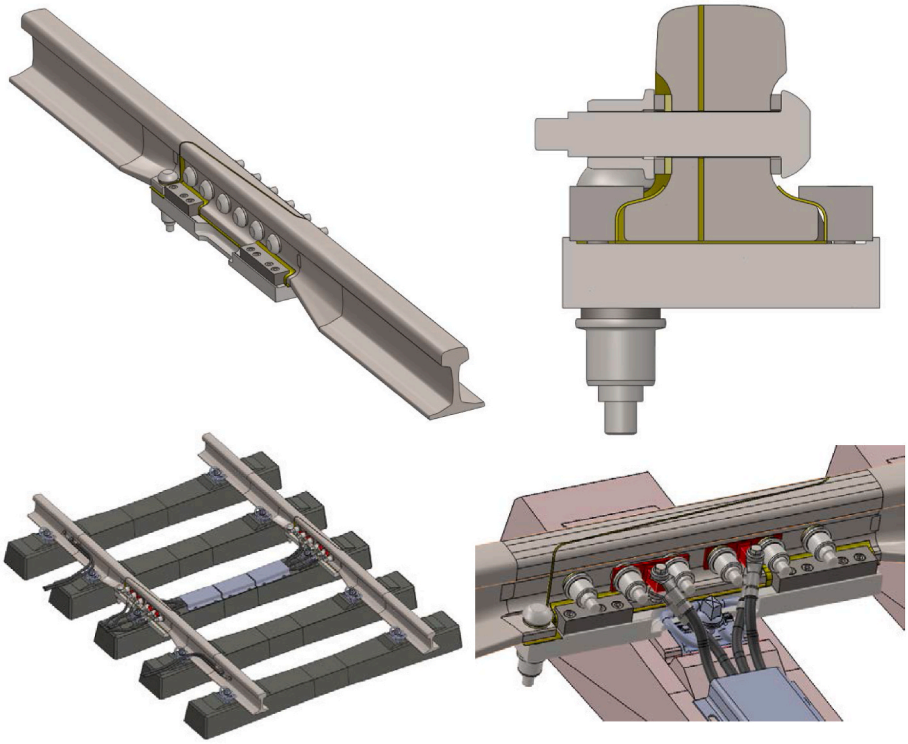

Fig. 5. Drawings of a "heavy" version of ABJ with 6 bolts and additional clamps to constrain the rails to the joint cover. Top left: general view. Top right: Cross section at the first lockbolt. Large web thick size can be appreciated. Bottom left: installation in a track with standard rail fasteners, standard sleepers and sleeper spacing. Bottom right: close-up of the cabling using stainless steel elements and bolts as conductors that completely free the tamping area.

specimens of single-lap bonded joints with a single bolt connection and external loads usually below 10 kN. Generally, results show that the higher the thickness of the adherend and adhesive, the applied load and the strength of bolts, the higher the load transferred by bolts, which increases also with the decrease of the adhesive shear modulus [29–32]. Therefore, the simplified hypothesis that the strength provided by bolts preload and the shear strength of the glue simply add can be reasonably considered for IRJs.

Accurate structural validations of ABJ were performed by a FEA model for both static and fatigue behaviour leading to a configuration satisfying all the requirements under heavy loads (40 t/axle).

The detailed description of the fully non-linear FEA model and its results lie outside the scope of this paper. It included bolts pretensioning, contact management and non-linear mechanical properties of high strength epoxy glue and insulating layers (Fig. 6).

3. Wheel-rail interaction of conventional IRJs and the innovative ABJ

3.1. Available IRJ wheel-rail interaction models

As the most common joint degradation mechanisms are plastic deformation of railheads in the end post and damages due to wheel-rail shocks in the same area, a detailed analysis of the wheel-rail contact interaction in this area is needed.

The bending stiffness discontinuity in a conventional IRJ can be idealized as a dip angle irregularity α, which generates impact forces (P_1) and low frequencies forces (P_2) greater than the static wheel load (P_0) when the vehicle runs on it.

The impact force P_1 does not depend linearly on track and vehicle parameters. Jenkins [33] provides an approximated formulation (1) where the impact force is calculated from dip angle value α, vehicle

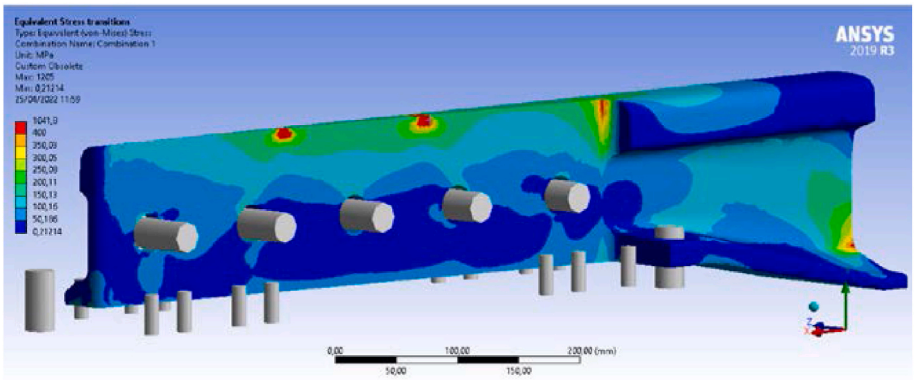

Fig. 6. FEA modelling of ABJ under fatigue bending. Stresses on a switch rail are shown. The "red stress dots" on the upper surface are due to the local effect of the applied vertical forces. (For interpretation of the references to colour in this figure legend, the reader is referred to the Web version of this article.)

speed V, effective track mass m_e (calculated as 0.4 m, with m the sum of rail mass m_r and the half sleepers mass m_s per unit length), the vehicle unsprung mass m_u and the Hertz spring constant K_H. The latter can be usually assumed 1.5*10^9 N/m depending on material properties (Young modulus and Poisson's ratio), wheel and rail radii and wheel load. The graphic representation of the formulation is shown in Fig. 7.

$$P_1 = P_0 + 2\alpha V\sqrt{\frac{K_H m_e}{1 + m_e/m_u}} \tag{1}$$

Other approaches to the estimation of the effect of dip angle irregularities include two- and three-dimensional models of the vehicle-track interaction in the presence of joints. A three-dimensional model is presented in Ref. [34] to develop a simplified equation for impact forces prediction, obtaining similar values ($P_1 = 1.05$–$1.66\ P_0$, $P_2 = 1.03$–$1.30\ P_0$), that depends on the vehicle speed ($V = 25$–100 km/h) and the dip angle of the irregularity ($\alpha = 0.8$–2.4 mrad), i.e. $2\alpha V$ values between 0.01 and 0.13.

A parametric study of the vehicle-track interaction using a two-dimensional model is described in Ref. [35], showing that the P_1 force also depends on the shape of the irregularity and not only on the value of the joint angle. Nevertheless, unsprung mass and joint angle are the main parameters influencing the impact force.

It can be concluded from all the sources available in the literature that the impact force cannot be eliminated by working on the geometry of conventional IRJs.

3.2. IRJ and ABJ model description and tuning

In combination with material constitutive models, FEA can predict localized ratcheting and lipping of the rail edge at the end post location of IRJs [36,37]. To pursue this goal, both static and dynamic non-linear FEA models of ABJ and IRJ were developed in this research to investigate and compare their behaviour under vertical wheel loads in both low and high-speed conditions.

The FEA model (Fig. 8) uses 3D elements for the central part that includes the detailed joint geometry and 1D beam elements for the external parts, with an overall length of 9.0 m for the IRJ (suspended between two sleepers) and 9.6 m for the ABJ (supported by a sleeper). The rail is supported by spring elements with a vertical stiffness of $k_z =$ 20 kN/mm simulating the influence of both the railpad and the ballast.

The model for the static analysis considers loads (vertical forces) directly applied on the rail, while in the dynamic analyses a load of 98.1 kN (10 t wheel load) was applied by half of the wheelset mass (unsprung mass = 750 kg), one quarter of bogie mass (simply sprung mass = 2000 kg) and one eight of carbody mass (double sprung mass = 7250 kg). These parameters are typical of an 80 tonnes locomotive, with two bogies with a mass of 11 tonnes each.

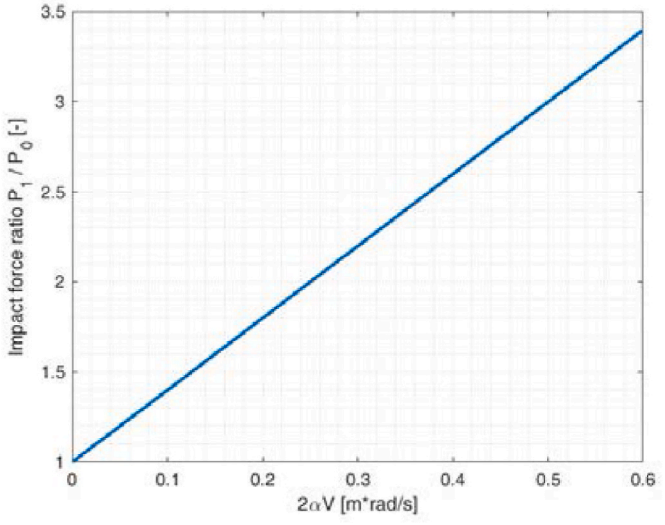

Fig. 7. Impact force ratio according to Jenkins approximated formulation [33].

A 940 mm diameter wheel was modelled to generate the wheel-rail contact, with a friction coefficient $f = 0.3$. The masses are connected by a primary spring with a stiffness $k_p = 1000$ N/mm and a secondary spring with a stiffness of $k_s = 450$ N/mm 60E1 profile is used for the rail, while the wheel has a simplified conical profile.

Contact stress analysis was performed by finely meshing the bodies at the wheel-rail contact position for the dynamic analysis (Fig. 8), to reproduce the Hertzian contact in the static position. The accuracy of the model was checked by comparing the numerical results of the contact pressure distribution to Hertz theory (2) where p_0 is the maximum Hertzian pressure, a and b are the semi-axes of the elliptic contact area in the x (rolling) and y (transverse) directions and N is the normal load. The semi-axes can be calculated using look-up tables or in closed form according to Ref. [39].

$$p = p_0\left(1 - \left(\frac{x}{a}\right)^2 - \left(\frac{y}{b}\right)^2\right)^{1/2}$$

where

$$p_0 = \frac{3N}{2\pi ab} \tag{2}$$

A test load of 100 kN resulted in $p_0 = 1190$ MPa, $a = 7.6$ mm and $b =$ 5.3 mm. Fig. 9 shows that smaller element sizes provide a better agreement with Hertz's theory. Cubic elements with 2 mm edge size were chosen as they resulted in an error of 2.5% in terms of maximum contact pressure.

3.3. Behaviour under quasi-static loads

This section compares the behaviour of conventional IRJ to ABJ in terms of stresses, contact forces and displacements under quasi-static loading. As horizontal stiffness is very similar for both IRJ and ABJ and no particular differences are expected, the attention was focused on the vertical stiffness as while that of IRJ dramatically drops at the end post location, the ABJ shows a more uniform stiffness along the entire transition. The cross-section moments of inertia J_{yy} and J_{zz} along the rail axis are shown in Fig. 10.

The IRJ was then simulated under vertical loads in a common condition for this kind of joint, i.e. with the joint suspended (midplane $x =$ 0 coincident with the midspan of the sleepers), while the ABJ was simulated in its design condition, i.e. supported by a sleeper (midplane x = 0 over the sleeper). Both models were subjected to an exceptional static vertical load of 200 kN (≈40 t/axle) applied in the midplane $x = 0$, resulting in a rail deflection of −2.73 mm for IRJ and of −2.47 mm for ABJ (Fig. 11).

Despite a large moment of inertia differences, the ABJ provides a static deflection that is only 9% smaller than that of the IRJ. This is because global deflection, related to the double integral of $M(x)/EJ(x)$ along the whole joint, is affected in a limited way by local large stiffness variations. It may be concluded that acting on joint stiffness leads by itself to only limited advantages.

The IRJ shows a rather pronounced dip angle in the end post area (α = 1.6 mrad) as the first derivative of elastic displacement of a beam is the first integral of the $M(x)/EJ(x)$ which is much more sensitive to local variations of the moment of inertia. As expected, the ABJ does not show this feature at all.

About stresses in the various components of the joints, the maximum Von Mises stress (318 MPa) appears in the fishplates for the IRJ while in the ABJ it appears in the joint cover with values (102 MPa) very close to those for the plain rail (in the order of 105 MPa over a sleeper).

The analyses above were repeated by slowly moving the load along

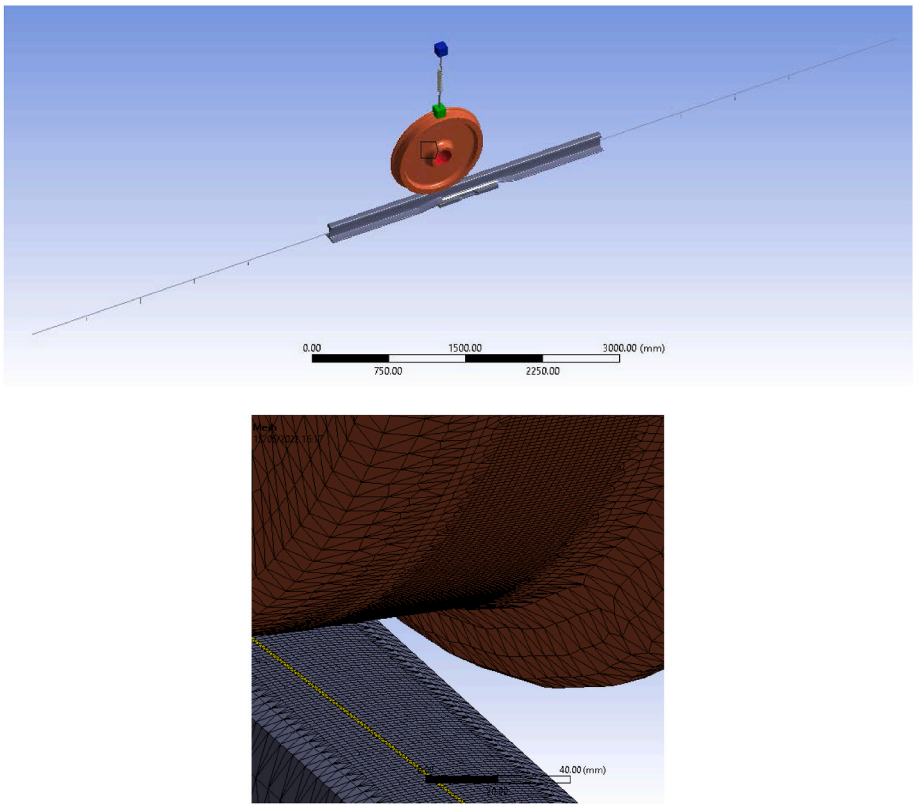

Fig. 8. Top: FEA model of a loaded wheel running over an ABJ. Green and blue blocks represent the bogie mass and the carbody mass respectively. In this frame the wheel is entering the ABJ with the prescribed speed. Bottom: detail of the mesh at the wheel rail contact for the ABJ (the yellow strip being the insulating fiberglass sheet separating the two half-joints). (For interpretation of the references to colour in this figure legend, the reader is referred to the Web version of this article.)

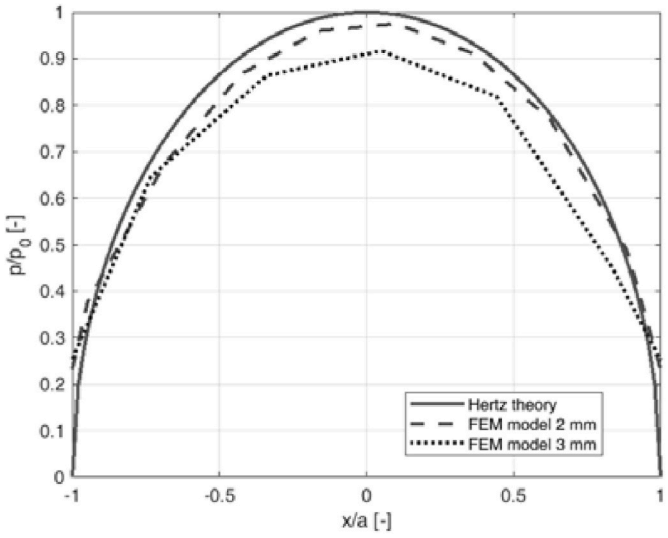

Fig. 9. Contact pressure distribution along the longitudinal axis from Hertz theory and FEA model with different of element size for meshing.

the model, comparing deflections with those appearing over a sleeper of the standard track and maximum stresses (Fig. 12). While for ABJ the maximum stress is always in the rails (not in the joint cover), the maximum stress for IRJ was found in the fishplates when the load is applied in the $x = 0$–200 mm and the rail for $x > 200$ mm. This explains why fishplates often break in service, especially in loosened joints.

The limited and smooth reduction of stiffness of ABJ in the forged transition leads to a negligibly greater rail deflection and stresses under wheel loads.

3.4. Behaviour under dynamic loads

Fully transient dynamic analyses were performed with the vehicle model passing over a conventional IRJ and ABJ at a constant speed ($V = 30.5$ m/s $= 110$ km/h) with an integration time step of 0.1 ms, i.e. with $\Delta x = 3$ mm.

In the case of IRJ, rails generate a dip angle $\alpha = 0.9$ mrad (Fig. 13) when the wheel is over the end post area ($x = 0$). Vertical displacement at the midplane is shown in Fig. 14 (left) as a function of the wheel position. Rail deformation initially increases while the wheel moves along the joint as the fishplates are not able to restore the correct geometry because of the gap. The gap generates a wheel/rail unloading with a consequent upward rail movement that is evident at $x = 0$ mm.

Wheel-rail contact conditions shown in Fig. 14 (right) highlight the resulting impact force P_1. The peak value of the force is about 121 kN, which results in a force increase of $P_1/P_0 = 1.23$, a value that is comparable to those described in Refs. [34,38] and with Jenkins formulation (1) for a value of $2\alpha V$=0.055. After the gap, the joint is loaded again reaching the largest displacement after further 180 mm while the vertical force increases again.

The ultimate goal of the ABJ was to completely avoid shocks as the shallow transition should have resulted in a longer transfer of the load between the two rails.

The behaviour under lateral loads was not analysed as an arbitrary cross-section along the axis shows a transverse profile that is identical to a railhead but for the thin insulating layer between the two half-joints. Under lateral loads, the wheel-rail contact is concentrated in the rail shoulder. It is worth noting that the ends of the inclined cuts are relatively thick and are not weak as in the milled portion of switch blades that are sharp cut instead. This feature, combined with a regular lateral

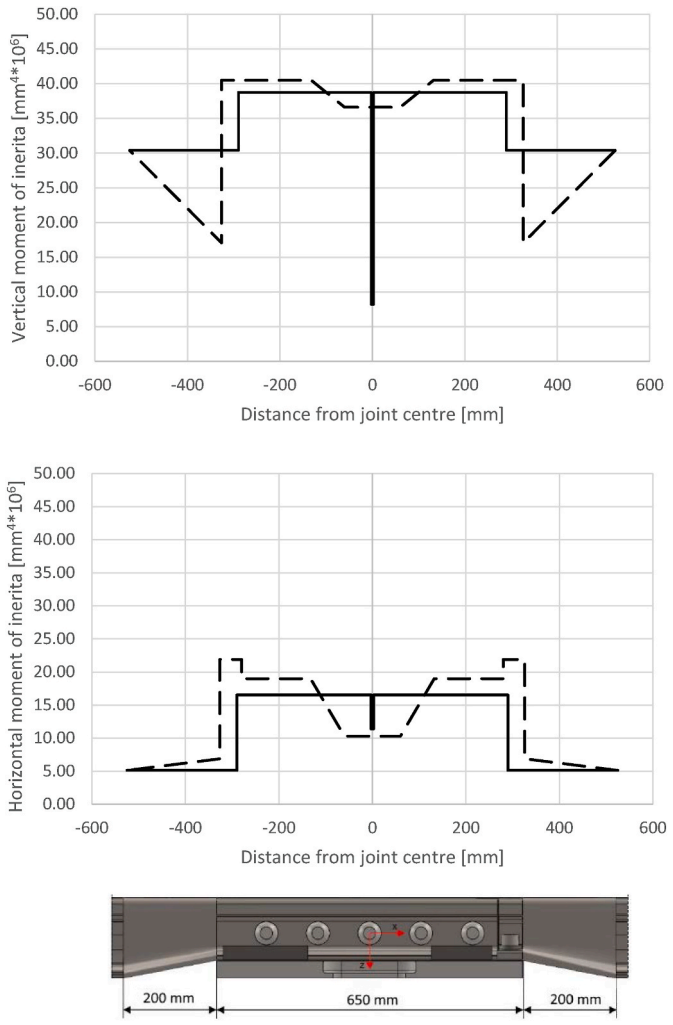

Fig. 10. Vertical (top) and horizontal (bottom) bending moment of inertia of IRJ (solid line) and ABJ (dashed line) along the rail axis. The limited overall length of the joint (1050 mm) is due to the need of using standard sleepers at both ends.

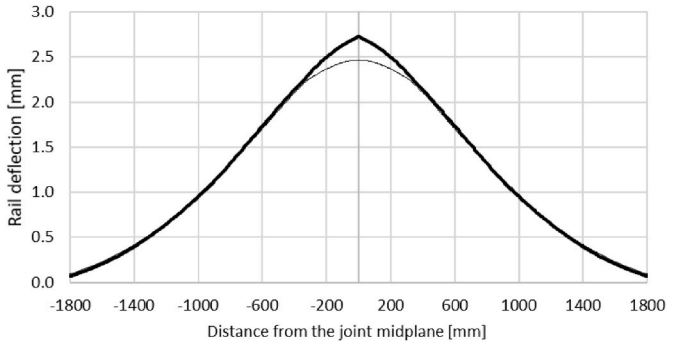

Fig. 11. Rail deflection of IRJ (thick line) and ABJ (thin line) under a 200 kN static load applied at the centre of the joint.

stiffness as shown above justifies the assumption that there should be no specific problems when the ABJ will be installed in curves.

Similarly, the effect of the heavier ABJ on vertical dynamics (vibrations) should be negligible. In Ref. [40] the effect of an increased mass is found beneficial for frequencies far from the pinned-pinned resonance. It should be reminded that some in-sleeper point machines have a mass of around 800 kg, i.e. over 3 times the mass of a concrete sleeper, and that their use similarly to even heavier components such as manganese steel casted crossings, generates very limited problems to running dynamics.

While the contact patch is split between the two rails depending on the actual wheel and rail profile coupling, the transition lasts in any case for much longer than for any conventional IRJ. In nominal conditions (new wheels and new rails) the contact is centred. As shown in Fig. 15, an elliptical contact patch with $a = 7.6$ mm, $b = 5.3$ mm results and the load transfer between the two rails is symmetrical w.r.t. the midplane of the joint, i.e. vertical force is equally shared between the two half-joints at $x = 0$ mm.

The length l_t needed to complete the transition is about 200 mm, much larger than the longitudinal size of the contact patch ($l_t/2a \approx 13$), while for square- or 45°-cut IRJ it is always shorter than the contact patch.

Vertical displacement of the ABJ measured at the midplane $x = 0$ mm (Fig. 16, left) highlights the absence of any discontinuities during the wheel pass-by. This results in a nearly constant vertical force at the passage over the joint (Fig. 16, right), that moreover withstands a sort of "handover" process between the half-joints resulting in a quiet and extremely smooth passage of the wheel over the joint.

If the contact point between wheel and rail is laterally shifted due to worn profiles or different rail inclination, the transition is not symmetrical with respect to the midplane of the joint, the length needed to complete the load transfer between the two rails is shorter and the fillet at the end of the cut is involved. In the example shown in Fig. 17 the transition length is about 60 mm and the transfer of the contact force between the half-joints is faster. Nevertheless, also in this case the transition can avoid impact forces and the wheel passage is much smoother than any IRJ.

The linear material model implemented in the present study does not allow a full analysis of the damages introduced by the repeated action of the impact forces, which is an important limitation of the present study.

Nevertheless, it was largely proven in the literature that the degradation of conventional IRJs is rapid, as shown in Ref. [41] where an exponential rule for rail ad fishplate stresses is given with respect to the concave depth of the irregularity generated at the sharply cut end post, only if impact forces can trigger the plastic deformation of steel.

For the ABJ, the absence of shocks does not lead to stresses exceeding yield stresses and fatigue is under control, also because the edges on the running surface could be easily chamfered. More sophisticated approaches involving advanced models of the elastoplastic behaviour of materials are therefore not needed as all the ABJ components work in the elastic domain.

4. Manufacturing and testing of the first ABJ prototype

The first ABJ prototype (Fig. 18) was assembled smoothly and without troubles during August 2022. This was an extremely tough phase as epoxy glue hardens in around 30 min (and cures completely in around 15 days), so no mistakes or uncertainties were allowed.

The joint was subjected to electrical resistance and electrical rigidity tests, while mechanical tests were limited to a 1450 kN (force arising for $\Delta T = 50$ °C in a 60 E1 CWR) pull-apart test according to the European standard [7] as the bending fatigue testing device was not available. All the tests were successfully passed.

These preliminary results were first shown during the CM2022 conference in Melbourne and the joint was then put on display at the Innotrans 2022 trade fair in Berlin.

5. Conclusions and further developments

The concept of an innovative insulated rail joint made by assembling standard rail components, named ABJ, was introduced in the paper.

Extensive numerical simulations with finite element analysis showed that the transition from one half-joint to the other is smooth for the ABJ

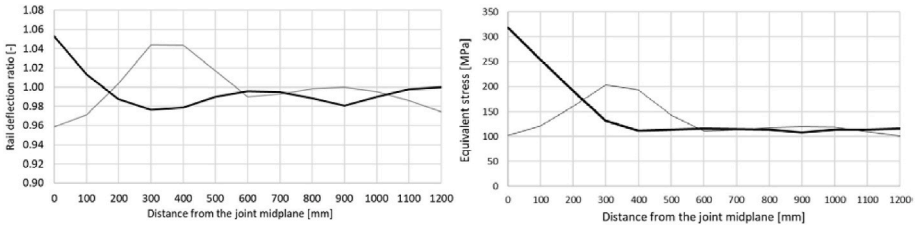

Fig. 12. Plot of displacements and maximum stress in the joints (IRJ = thick line, ABJ = thin line) seen by a slowly 200 kN moving load. Left: vertical rail deflection normalized to the behaviour over a sleeper for a standard track. Right: maximum equivalent stresses according to Von Mises criterion.

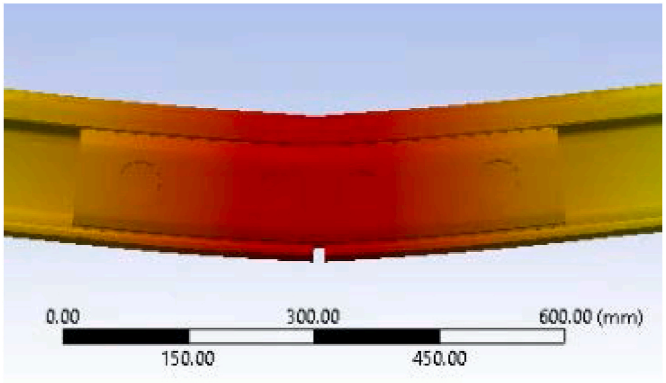

Fig. 13. 100× magnification of the vertical deflection of the joint when the wheel passes at x = 0.

and without the shocks typical of the conventional IRJ as the dip angle irregularity is eliminated by the new arrangement. This is the result of the combined effect of the long transition and the stiff reinforcing joint cover attached below the half-joints.

Long transitions exist in other railway products such as rail expansion joints and the switch rail/stock rail pair that are subject to less frequent and much less catastrophic failures than for IRJ. The reinforcing joint cover is instead an innovative feature in the railway field that is on the opposite widely used in bolted joints for civil structures to increase their bending stiffness. This thick plate fastened below the half-joints for the whole length of the transition prevents the generation of high shear stresses between the two half-joints when the joint is loaded, something that is impossible with fishplates of conventional IRJs regardless of stiffness and length of the fishplates.

As a result, the target of the design phase of the ABJ development project was fully achieved. Rail surface damages, cracks, failures, noise, vibrations and ballast degradation can be therefore prevented with the new arrangement. ABJ can be installed in any plain track with standard sleepers and standard rail fastening systems, allowing continuous track tamping.

Tests on the first prototype have proven the feasibility and strength of ABJ. The development plan will include a specific lab test campaign to validate the assumption of superposition of strength for bolted-bonded joints and define the final architecture to be used for the complete set of homologation tests that will be carried out at an accredited laboratory.

Immediately after homologation is received, the first samples to put in service will be manufactured and laid in a track. The current plan estimates this phase by the end of 2023.

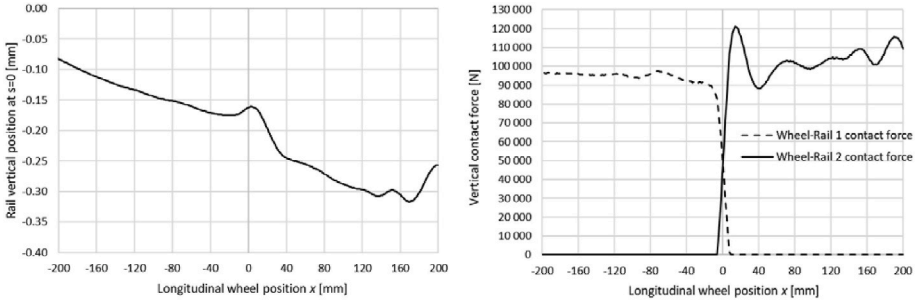

Fig. 14. Left: vertical displacement of IRJ at $x = 0$ during wheel pass-by. Right: vertical contact force between the wheel and the two rails of IRJ during wheel pass-by.

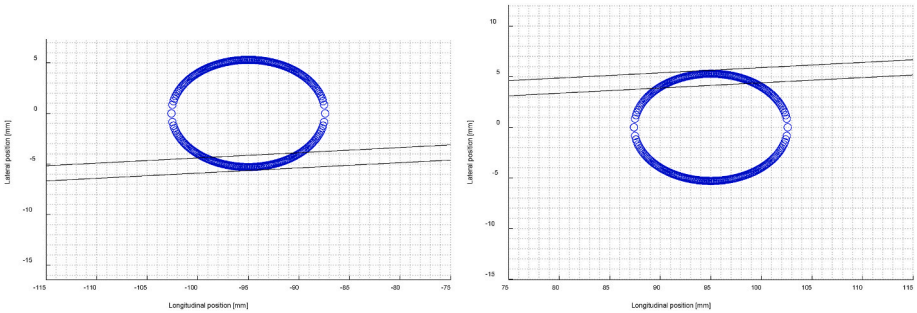

Fig. 15. Initial (left) and final (right) positions of the wheel-rail boundary contact patch.

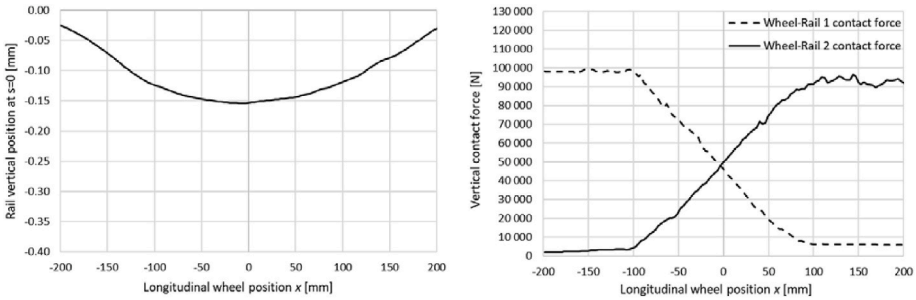

Fig. 16. Left: vertical displacement at the x = 0 during wheel pass-by. Right: vertical contact force between the wheel and the two half-joints of ABJ during wheel pass-by.

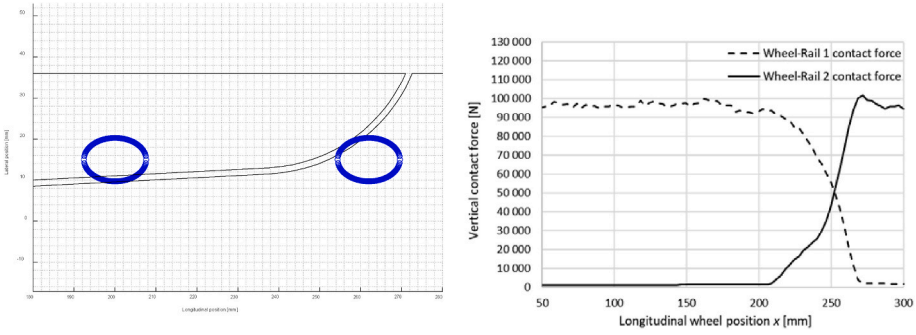

Fig. 17. Initial and final contact positions (left) and vertical contact force between the wheel and the half-joints during wheel pass-by (right) considering a 15 mm lateral shift of the wheel-rail contact.

Fig. 18. First ABJ prototype just after the assembly (left) and placed into the pull-apart machine (right).

Declaration of competing interest

The authors declare that they have no known competing financial interests or personal relationships that could have appeared to influence the work reported in this paper.

Data availability

No data was used for the research described in the article.

References

[1] N.K. Mandal, M. Spiryagin, Q. Wu, Z. Wen, S. Stichel, FEA of mechanical behaviour of insulated rail joints due to vertical cyclic wheel loadings, Eng. Fail. Anal. (2022) 133.
[2] M. Quirchmair, Optimising the track bedding stiffness and settlement behaviour at insulated rail joints, Rail Eng. Int. 4 (2020) 9–14.
[3] H. Elsayed, M. Lotfy, H. Youssef, H. Sobhy, Assessment of degradation of railroad rails: finite element analysis of insulated joints and unsupported sleepers, J. Mech. Mater. Struct. 14 (3) (2019 Oct 8) 429–448.
[4] T.X. Wu, D.J. Thompson, On the impact noise generation due to a wheel passing over rail joints, J. Sound Vib. 267 (2003) 485–496.
[5] H. Askarinejad, M. Dhanasekar, P. Boyd, R. Taylor, Field measurement of wheel–rail impact force at insulated rail joint, Exp. Tech. 39 (2015) 61–69.
[6] J. Xiao, Z. Yan, J. Shi, D. Ma, Effects of wheel-rail impact on the fatigue performance of fastening clips in rail joint area of high-speed railway, KSCE J. Civ. Eng. 26 (1) (2022 Jan 1) 120–130.
[7] prEN16843, Railway Applications - Infrastructure – Mechanical Requirements for Joints in Running Rails, CEN, Brussels, 2019, 2019.
[8] Ministry of Transport, Report on the Derailment that Occurred on 5th November, 1967, near Hither Green, London, 1968.
[9] https://en.wikipedia.org/wiki/Pioltello_train_derailment. (Accessed 24 February 2023).
[10] J. Stephen, C. Hardwick, P. Beaty, R. Lewis, M. Marshall, Ultrasonic monitoring of insulated block joints, Proc. Inst. Mech. Eng. F J. Rail Rapid Transit 233 (3) (2019 Mar) 251–261.
[11] M. Molodova, M. Oregui, A. Núñez, Z. Li, R. Dollevoet, Health condition monitoring of insulated joints based on axle box acceleration measurements, Eng. Struct. 123 (2016 Sep 15) 225–235.
[12] A. Mayers, The effect of heavy haul train speed on insulated rail joint bar strains, Aust. J. Struct. Eng. 18 (3) (2017 Jul 3) 148–159.
[13] E. Soylemez, K. Ciloglu, Influence of track variables and product design on insulated rail joints, Transport. Res. Rec.: J. Transport. Res. Board (2016) 2545 1–254510.
[14] M. Gallou, B. Temple, C. Hardwick, M. Frost, A. El-Hamalawi, Potential for external reinforcement of insulated rail joints, Proc. IMech.E Part F: J. Rail Rapid Transit. 232 (3) (2018) 697–708.
[15] N. Zong, M. Dhanasekar, Minimization of railhead edge stresses through shape optimization, Eng. Optim. 45 (9) (2013) 1043–1060.
[16] N. Zong, M. Dhanasekar, Experimental studies on the performance of rail joints with modified wheel/railhead contact, Proc. IMech.E Part F: J. Rail Rapid Transit. 228 (8) (2014) 857–877.
[17] M. Dhanasekar, Sleeper embedded insulated rail joints for minimising the number of modes of failure, Eng. Fail. Anal. 76 (2017) 27–43.
[18] Bosso N, Bracciali A, Megna G, Zampieri N. Effects of geometric track irregularities on vehicle dynamic behaviour when running through a turnout. Veh. Syst. Dyn., DOI: 10.1080/00423114.2021.1957127, published online: 30 July 2021.

[19] B. Yann, B.A. Pålsson, Multibody simulation benchmark for dynamic vehicle-track interaction in switches and crossings: modelling description and simulation tasks, Veh. Syst. Dyn. (2021), https://doi.org/10.1080/00423114.2021.1942079.
[20] H.M. El-sayed, M. Lotfy, H.N. El-din Zohny, H.S. Riad, A three dimensional finite element analysis of insulated rail joints deterioration, Eng. Fail. Anal. 91 (2018 Sep 1) 201–215.
[21] M. Dhanasekar, W. Bayissa, Performance of square and inclined insulated rail joints based on field strain measurements, Proc. IMech.E Part F: J. Rail Rapid Transit. 226 (2011) 140–155.
[22] S. Ataei, S. Mohammadzadeh, A. Miri, Dynamic forces at square and inclined rail joints: field experiments, J. Transport. Eng. 142 (9) (2016 Sep), 04016035.
[23] R.H. Plaut, H. Lohse-Busch, A. Eckstein, S. Lambrecht, D.A. Dillard, Analysis of tapered, adhesively bonded, insulated rail joints, Proc. IMech.E Part F: J. Rail Rapid Transit. (2007), 221-195.
[24] M.N. Akhtar, D.D. Davis, Preliminary Results of Prototype Insulated Joint Tests at FAST. Technology Digest TD-07-013, Association of American Railroads, Transportation Technology Center, Inc., 2007.
[25] D.D. Davis, M.N. Akhtar, Prototype Next Generation Insulated Joints. Technology Digest TD-10-009, Association of American Railroads, Transportation Technology Center, Inc., 2010.
[26] G. Megna, A. Bracciali, Smooth transition insulated rail joints, in: Proceedings of 12th International Conference on Contact Mechanics and Wear of Rail/Wheel Systems (CM2022), September 2022, pp. 4–7. Melbourne, Australia.
[27] World Patent Extension PCT/IB2023/053400 of the Italian Patent, Request Filed on 04.04, 2023.
[28] EN13674-2:2019, Railway Applications - Track - Rail - Part 2: Switch and Crossing Rails Used in Conjunction with Vignole Railway Rails 46 Kg/m and above, CEN, Brussels, 2019.
[29] G. Kelly, Load transfer in hybrid (bonded/bolted) composite single-lap joints, Compos. Struct. 69 (1) (2005 Jun) 35–43.
[30] K. Bodjona, L. Lessard, Load sharing in single-lap bonded/bolted composite joints. Part II: global sensitivity analysis, Compos. Struct. 129 (2015 Oct) 276–283.
[31] X. Li, X. Cheng, X. Guo, S. Liu, Z. Wang, Tensile properties of a hybrid bonded/bolted joint: parameter study, Compos. Struct. 245 (2020 Aug), 112329.
[32] A. Barut, E. Madenci, Analysis of bolted–bonded composite single-lap joints under combined in-plane and transverse loading, Compos. Struct. 88 (2009 May 1) 579–594.
[33] H.H. Jenkins, J.E. Stephenson, G.A. Clayton, et al., The effect of track and vehicle parameters on wheel/rail vertical dynamic forces, Railw. Eng. J. 3 (1) (1974) 2–16.
[34] N.K. Mandal, M. Dhanasekar, Y. Quan Sun, Impact forces at dipped rail joints, Proc. IMech.E Part F: J. Rail Rapid Transit. 230 (1) (2016) 271–282.
[35] I. Grossoni, S. Iwnicki, Y. Bezin, C. Gong, Dynamics of a vehicle–track coupling system at a rail joint, Proc. IMech.E Part F: J. Rail Rapid Transit. 229 (4) (2015) 364–374.
[36] J. Sandström, A. Ekberg, Numerical study of the mechanical deterioration of insulated rail joints, Proc. IMech.E Part F: J. Rail Rapid Transit. 223 (2009) 265–273.
[37] N.K. Mandal, FEA to assess plastic deformation of rail head material damage of insulated rail joints with fibre glass and nylon end posts, Wear (2016) 366–367, 3-12.
[38] T. Pang, M. Dhanasekar, Dynamic finite element analysis of the wheel – rail interaction adjacent to the insulated rail joints, in: Proceedings of 7th International Conference on Contact Mechanics and Wear of Wheel/Rail Systems (CM2006), September 2006, pp. 24–26 (Brisbane, Australia).
[39] A.A. Shabana, M. Berzeri, J.R. Sany, Numerical procedure for the simulation of wheel/rail contact dynamics, J. Dyn. Syst. Meas. Control 123 (2) (2001) 168–178.
[40] A. Bracciali, M. Macherelli, F. Piccioli, Rail vibrations: data analysis and FE modelling with applications to signalling equipment, in: Proceedings of the Second International Conference on Railway Technology: Research, Development and Maintenance, Ajaccio, Corsica, 8-11 April 2014, https://doi.org/10.4203/ccp.104.200.
[41] H. Xiao, G. Liu, D. Yan, Y. Zhao, J. Wang, H. Wang, Field test and numerical analysis of Insulated rail joints in heavy-haul railway, Construct. Build. Mater. 298 (2021 Sep), 123905.